ESC European Society of Cardiology

Europace (2023) **25**, 1–7
https://doi.org/10.1093/europace/euad211

CLINICAL RESEARCH

Feasibility of three-dimensional artificial intelligence algorithm integration with intracardiac echocardiography for left atrial imaging during atrial fibrillation catheter ablation

Luigi Di Biase [1]*†, Fengwei Zou [1†], Aung N. Lin[1], Vito Grupposo[2], Jacopo Marazzato [1,3], Nicola Tarantino[1], Domenico Della Rocca [4], Sanghamitra Mohanty[4], Andrea Natale [4], Majd Al Deen Alhuarrat [1], Guy Haiman [2], David Haimovich [2], Richard A. Matthew [2], Jaclyn Alcazar [2], Graça Costa [2], Roy Urman[2], and Xiaodong Zhang [1]

[1]Montefiore-Einstein Center for Heart & Vascular Care, Department of Cardiology, Montefiore Medical Center, Albert Einstein College of Medicine, 111 E 210th street, Bronx, NY, USA; [2]Biosense Webster, Inc., Irvine, CA, USA; [3]Department of Medicine and Surgery, University of Insubria, Varese, Italy; and [4]St. David's Medical Center, Texas Cardiac Arrhythmia Institute, Austin, TX, USA

Received 18 March 2023; accepted after revision 10 July 2023; online publish-ahead-of-print 21 July 2023

Aims

Intracardiac echocardiography (ICE) is a useful but operator-dependent tool for left atrial (LA) anatomical rendering during atrial fibrillation (AF) ablation. The CARTOSOUND FAM Module, a new deep learning (DL) imaging algorithm, has the potential to overcome this limitation. This study aims to evaluate feasibility of the algorithm compared to cardiac computed tomography (CT) in patients undergoing AF ablation.

Methods and results

In 28 patients undergoing AF ablation, baseline patient information was recorded, and three-dimensional (3D) shells of LA body and anatomical structures [LA appendage/left superior pulmonary vein/left inferior pulmonary vein/right superior pulmonary vein/right inferior pulmonary vein (RIPV)] were reconstructed using the DL algorithm. The selected ultrasound frames were gated to end-expiration and max LA volume. Ostial diameters of these structures and carina-to-carina distance between left and right pulmonary veins were measured and compared with CT measurements. Anatomical accuracy of the DL algorithm was evaluated by three independent electrophysiologists using a three-anchor scale for LA anatomical structures and a five-anchor scale for LA body. Ablation-related characteristics were summarized. The algorithm generated 3D reconstruction of LA anatomies, and two-dimensional contours overlaid on ultrasound input frames. Average calculation time for LA reconstruction was 65 s. Mean ostial diameters and carina-to-carina distance were all comparable to CT without statistical significance. Ostial diameters and carina-to-carina distance also showed moderate to high correlation ($r = 0.52$–0.75) except for RIPV ($r = 0.20$). Qualitative ratings showed good agreement without between-rater differences. Average procedure time was 143.7 ± 43.7 min, with average radiofrequency time 31.6 ± 10.2 min. All patients achieved ablation success, and no immediate complications were observed.

Conclusion

DL algorithm integration with ICE demonstrated considerable accuracy compared to CT and qualitative physician assessment. The feasibility of ICE with this algorithm can potentially further streamline AF ablation workflow.

* Corresponding author. Tel: +1 718 920 4321. *Email address*: dibbia@gmail.com

† The first two authors contributed equally to the study and are co-first authors.

Graphical Abstract

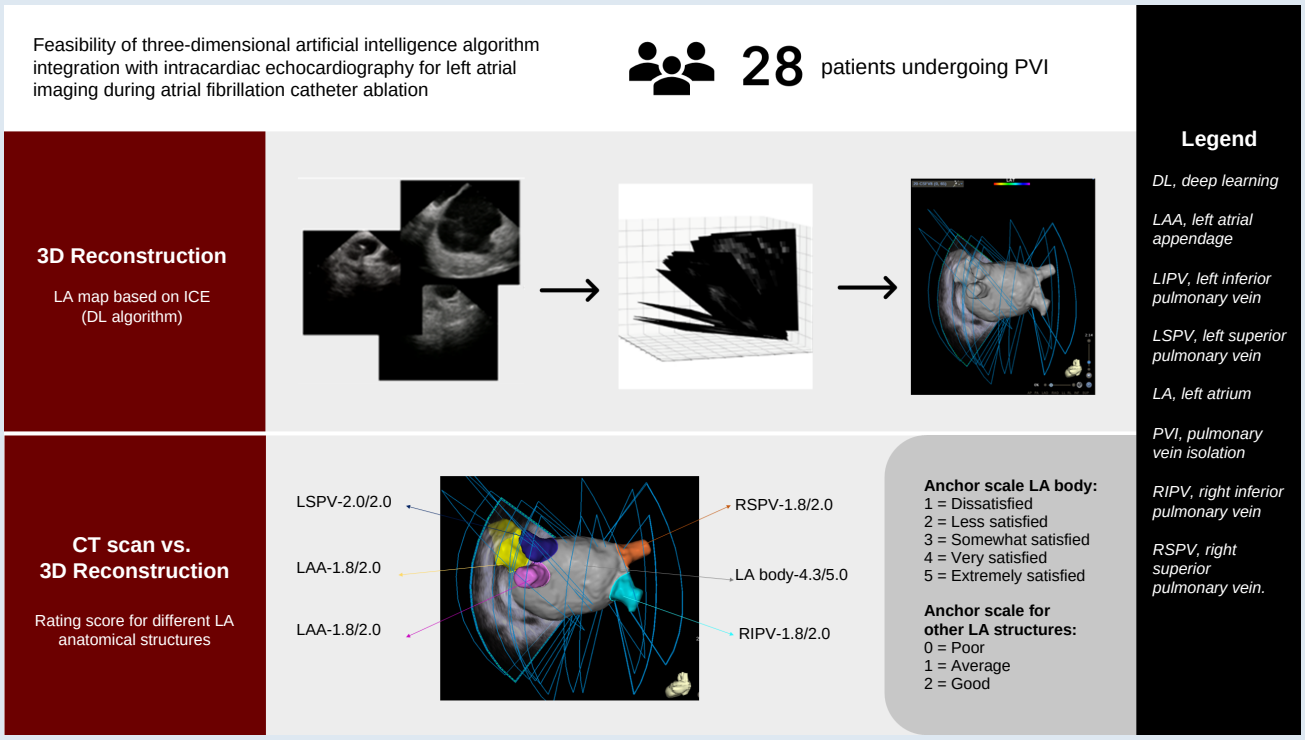

Keywords Atrial fibrillation • Catheter ablation • Intracardiac echocardiography • Deep learning • Artificial intelligence

What's new?

- The three-dimensional (3D) rendering of the left atrium (LA) by multi-electrode catheters on top of 3D mapping systems is now considered the standard of care to guide catheter ablation of atrial fibrillation.
- Although the intracardiac echocardiography (ICE) already proved to be helpful in guiding a pulmonary vein isolation procedure (PVI), the evidence on 3D reconstruction of the LA based on ICE is scarce.
- This is the first study to describe the feasibility of a new novel deep learning algorithm based on ICE to create a non-contact 3D rendering of the LA during the PVI workflow.
- Before trans-septal puncture and without the need of any multipolar catheter in the LA, the 3D rendering of the LA based on an ICE algorithm yielded similar results to computed tomography scan acquisitions. However, broader studies are required to investigate the applicability of this new technique during PVI.

Introduction

Intracardiac echocardiography (ICE) has been vastly incorporated in the current atrial fibrillation (AF) catheter ablation workflow over the past decade. Technological advancement has yielded ICE an essential tool to delineate left atrial (LA) anatomy, rule out LA appendage (LAA) thrombus, detect pericardial effusion, and perform fluoroless ablations. Recently, some studies have demonstrated the feasibility of reconstructing LA anatomy either with ICE alone or by merging with cardiac computed tomography (CT) to guide cryoballoon or radiofrequency (RF) ablation.[1–6] Despite these benefits of ICE, one of the challenges found upon use of ICE lies within the increased time to image the full LA especially with lack of operator experience. As artificial intelligence (AI) is increasingly applied to the field of electrophysiology in the past years, there is a need to automate the process of acquiring LA anatomy with ICE to create more accurate and reproducible anatomical maps to guide ablation. The CARTOSOUND™ FAM Module (Biosense Webster, Irvine, California, USA) is a deep learning (DL) algorithm aimed to automatically construct detailed three-dimensional (3D) LA anatomy. It utilizes two-dimensional (2D) ultrasound (ULS) clips acquired with the SOUNDSTAR™ Catheter (Biosense Webster, Irvine, CA, USA) positioned in the right atrium (RA) and/or the right ventricular outflow tract (RVOT). This study aims to evaluate feasibility and accuracy of the algorithm compared to cardiac CT in patients undergoing AF ablation in a high-volume US centre.

Methods

The deep learning module

The CARTOSOUND™ FAM Module is an automated version of the legacy CARTOSOUND™ Module. It is intended to simplify the workflow of cardiac anatomies mapping using the previous ULS technology by eliminating the need for the manual contouring process and by providing an enhanced fast anatomical mapping (FAM) workflow. The module incorporates an automatic algorithm, developed by Siemens Healthineers AG (Erlangen, Germany) that enables automatic detection of the cardiac anatomies using a series of 2D ULS input of the LA imaged anatomies. The DL algorithm is trained during the development phase and then deployed in a locked mode that does not learn during use. To create a prediction detector that can generate 3D segmentation from a sparse input volume, we train an image-to-image deep neural network to learn the detector parameters.

In the training phase, the network takes as an input the 3D sparse volume and the 3D ground truth. The output is way that minimizes the error between the predicted results computed by the network and the 3D ground truth provided as an input. Sparse volume reconstruction aims at collecting all the 2D input frames, mapping them to a 3D co-ordinate system, and finding the 3D volume that enclose all the inputs.

The module is currently limited for LA mapping only and does not support LA uncommon anatomical variations [e.g. 5th pulmonary vein (PV)]. The LA algorithm uses a series of 2D ULS input frames acquired from the RA (fossa ovalis) and the RVOT to (i) create a 3D volume reconstruction of the LA body, LAA, left superior PV (LSPV), left inferior PV (LIPV), right superior PV (RSPV), and right inferior PV (RIPV); (ii) provide 3D auto-segmentation for the relevant anatomical structures; (iii) generate 2D auto-contours that are overlaid on the corresponding 2D ULS frame; and (iv) provide 2D auto-tagging for the relevant anatomical structures. The map created is a standard FAM that can be further edited using existing FAM tools with magnetic sensor-based navigational catheters and for acquiring electro-anatomical data (*Figures 1* and *2*).

Study design

A total of 28 patients undergoing AF RF ablation in a single high-volume US centre were included in this study. All patients received pre-procedural cardiac CT. On day of ablation, standard AF ablation procedures were implemented, and patients underwent general anaesthesia. After vascular access is obtained, the ICE catheter was advanced to the RA and/or RVOT. Three-dimensional shells of LA body and adjacent anatomical structures including LAA, LSPV, LIPV, RSPV, and RIPV were reconstructed using the DL algorithm. The selected frames within the ULS clips were gated to the end-expiration phase and to the LA max volume. The results of the DL algorithm were evaluated by comparing the reconstructed anatomical structures to cardiac CT images. Computed tomography registration error was computed as the distance between map points and its closest CT image points after surface registration using the CARTOMERGE module (Biosense Webster, Irvine, CA, USA). The ostial diameter of cylindrical anatomical structures including the LAA, LSPV, LIPV, RSPV, RIPV, and carina-to-carina distance between the left and right PVs was recorded by both the DL algorithms, and pre-procedural CT and was measured manually by an experienced technical support staff and compared. Three independent experienced electrophysiologists also rated how accurately the DL algorithm delineated these anatomical structures. For LA adjacent anatomical structures, a three-anchor scale was used (0 = poor, 1 = average, 2 = good). For LA body, a five-anchor scale was used (1 = dissatisfied, 2 = less satisfied, 3 = somewhat satisfied, 4 = very satisfied, 5 = extremely satisfied).

Relevant baseline patient demographics, comorbidities, AF type, and medication use were recorded. Ablation-related characteristics including ablation time, RF time, number of RF applications, types of ablations performed, and immediate complications were also summarized.

Acute ablation success is defined as conduction block in/out of each PV for PV isolation (PVI) and absence of any electrical potentials in ablation of non-PV triggers at end of ablation. Best practice recommendations of using the DL algorithm have also been collected and summarized.

Statistical analysis

Continuous variables were expressed as mean ± standard deviation. Discrete numerical scores were expressed as median and inter-quartile range (IQR). Scoring differences between raters were analysed using the non-parametric Friedman test that compared between three and five numerical scores given to the same object. Correlations between raters were analysed using the Kappa coefficients for each pair of raters. Paired *t*-test was used to compare the means between anatomical measurements obtained from CARTOSOUND FAM and cardiac CT. The Pearson correlation test was used to evaluate the correlation between these two groups. *P*-values of <0.05 were considered statistically significant.

Results

Baseline patient characteristics are presented in *Table 1*. The average age for the 28 patients enrolled in this study was 64.5 ± 9.9 years with 53.6% being male and mean congestive heartfailure, hypertension, age>75, diabetes, stroke, vascular disease, age 65-74, and sex category (gender) (CHA_2DS_2-VASc) score of 2.8 ± 1.5. A close to equal mix had paroxysmal vs. persistent AF (53.6% vs. 42.9%). Five patients (17.9%) also had concurrent atrial flutter. The average left ventricular ejection fraction was 54.0 ± 17.6%. All patients were in sinus rhythm at the start of ablation.

The DL algorithm generated both 3D volume reconstructions of the LA anatomies (LA body, LAA, LSPV, LIPV, RSPV, and RIPV) along with 2D contours that were overlaid on the corresponding 2D ULS frames. The average number of frames used by the algorithm to detect LA structures were as follows: LA—15.3, LIPV—1.4, LSPV—1.8, RIPV—2.8, RSPV—3.2, LAA—4.5. The overall lowest number of frames were 30 (IQR 25–34), while the highest number of frames were 31 (IQR 27–39). The average calculation time for the algorithm to reconstruct LA anatomies was 65 s. A

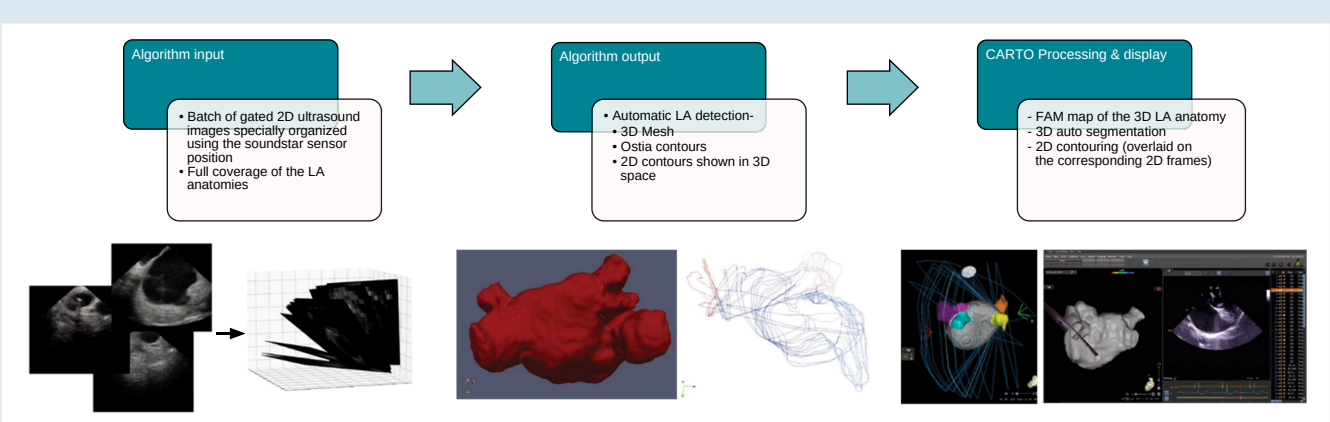

Figure 1 Deep learning algorithm data input flow diagram. Batches of two-dimensional (2D) ultrasounds gated frames covering the full left atrial (LA) anatomy and spatially organized using the intracardiac echocardiography (ICE) catheter position were imported into the deep learning algorithm. Automatic detection of the three-dimensional (3D) LA body and the adjacent anatomical structures [LA appendage (LAA), left superior pulmonary vein (LSPV), left inferior pulmonary vein (LIPV), right superior pulmonary vein (RSPV), and right inferior pulmonary vein (RIPV)] were performed along with the ostia, and the 2D contours were constructed. Fast anatomical mapping (FAM) of the 3D LA anatomy with 3D auto-segmentation, the 2D overlaying contours, and the 2D auto-taggings were shown as the final output on the mapping workstation.

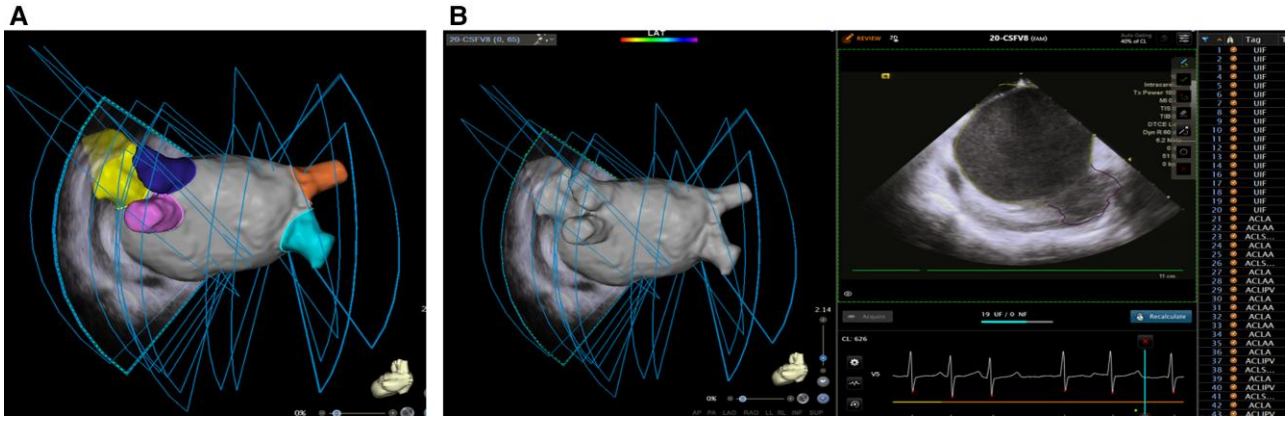

Figure 2 Three-dimensional (3D) reconstruction of left atrium (LA) and adjacent anatomies and automatic two-dimensional (2D) contour detection. (*A*) 3D reconstruction and auto-segmentation of overall LA shell and its adjacent structures including LA appendage (LAA) and pulmonary veins (PVs). (*B*) Automatic artificial intelligence (AI) 2D contour detection of the LA shell (yellow lines) and the LAA (purple line) and the 2D auto-tagging indicated on the right list.

Table 1 Patient characteristics

Parameters	*N* = 28
Age	64.5 ± 9.9
Male gender	15 (53.6%)
AF type	
Paroxysmal	15 (53.6%)
Persistent	12 (42.9%)
Atrial flutter	5 (17.9%)
Coronary artery disease	5 (17.9%)
Diabetes	8 (28.6%)
Dyslipidaemia	17 (60.7%)
Hypertension	21 (75.0%)
BMI	30.8 ± 6.2
Stroke or TIA	2 (7.1%)
CHA_2DS_2-VASc	2.8 ± 1.5
Oral anticoagulant use	
Apixaban	19 (67.9%)
Rivaroxaban	8 (28.6%)
Coumadin	1 (3.6%)
Beta-blocker use	24 (88.9)
Antiarrhythmic use	5 (17.9%)
Amiodarone	1 (3.6%)
Flecainide	3 (2.4%)
Propafenone	1 (3.6%)
LVEF (%)	54.0 ± 17.6

AF, atrial fibrillation; BMI, body mass index; TIA, transient ischaemic attach; LVEF, left ventricular ejection fraction.

Table 2 Ablation characteristics

Parameters	*N* = 28
Procedure time (min)	143.7 ± 43.7
Fluoroscopy time (min)	10.0 ± 8.7
RF time (min)	31.6 ± 10.2
Number of energy applications	87.8 ± 31.2
PVI	26 (92.9%)
PWI	23 (82.1%)
LAAEI	5 (17.9%)
SVC isolation	10 (35.7%)
CS isolation	7 (25.0%)
CTI	3 (10.7%)
Acute success	28 (100%)
Immediate complications	0 (0%)

RF , radiofrequency; PVI, pulmonary vein isolation; PWI, posterior wall isolation; LAAEI, left atrial appendage electrical isolation; SVC, superior vena cava; CS, coronary sinus; CTI, cavotricuspid isthmus.

newer version of the DL algorithm resulted in an improved average calculation time for reconstruction of LA anatomies at 25 s.

The average AF ablation procedure time was 143.7 ± 43.7 min, with average RF time 31.6 ± 10.2 min and 87.8 ± 31.2 energy applications. Most patients (92.9%) received PVI and posterior wall isolation (PWI, 82.1%). Other ablation lesion sets included LAA electrical isolation, superior vena cava isolation, coronary sinus (CS) isolation, and cavotricuspid isthmus isolation. All patients achieved acute ablation success, and no immediate complications were observed (*Table 2*).

The ostial diameter of cylindrical anatomical structures including the LAA, LSPV, LIPV, RSPV, and RIPV as well as carina-to-carina distance between the left and right PVs recorded by both the DL algorithm and pre-procedural CT was reported in *Table 3*. Mean ostial diameters and carina-to-carina distance were all comparable to CT without statistical significance. The Pearson correlation coefficients of LSPV, LIPV, RSPV, LAA, and carina-to-carina measurements also showed moderate to high correlation between the DL algorithm and CT. Deep learning algorithm measurements of RIPV showed relatively lower correlations with CT.

Comparisons between the overlaid contours generated by the DL algorithm also showed qualitative good agreement across the three

Table 3 Diameter of CARTOSOUND FAM anatomical structures vs. pre-procedural computed tomography (mm)

	CARTOSOUND FAM	CT	*P*-value	Pearson correlation coefficient (*r*)
LSPV	18.8 ± 4.4	20.0 ± 4.4	0.071	0.75
LIPV	16.9 ± 3.8	18.6 ± 3.3	0.054	0.52
RSPV	21.0 ± 3.5	22.0 ± 4.3	0.105	0.61
RIPV	19.1 ± 3.4	18.5 ± 3.4	0.596	0.20
LAA	25.6 ± 5.1	24.4 ± 5.8	0.076	0.54
Carina-carina distance	62.9 ± 3.3	61.9 ± 3.5	0.102	0.59

CT, computed tomography; LSPV, left superior pulmonary vein; LIPV, left inferior pulmonary vein; RSPV, right superior pulmonary vein; RIPV, right inferior pulmonary vein; LAA, left atrial appendage.

Table 4 Comparison of score differences between raters

LA structure	Rater	Mean	IQR	*P*-value
LSPV	Rater 1	2.00	2.00–2.00	1
	Rater 2	2.00		
	Rater 3	2.00		
	Median	2.00		
LIPV	Rater 1	1.89	1.89–1.91	0.875
	Rater 2	1.89		
	Rater 3	1.93		
	Median	1.89		
RSPV	Rater 1	1.82	1.75–1.82	0.345
	Rater 2	1.82		
	Rater 3	1.68		
	Median	1.82		
RIPV	Rater 1	1.82	1.82–1.82	1
	Rater 2	1.82		
	Rater 3	1.82		
	Median	1.82		
LAA	Rater 1	1.75	1.75–1.75	1
	Rater 2	1.75		
	Rater 3	1.75		
	Median	1.75		
Overall LA shell	Rater 1	4.32	4.31–4.32	0.972
	Rater 2	4.32		
	Rater 3	4.29		
	Median	4.32		

IQR, inter-quartile range; LA, left atrium; LSPV, left superior pulmonary vein; LIPV, left inferior pulmonary vein; RSPV, right superior pulmonary vein; RIPV, right inferior pulmonary vein; LAA, left atrial appendage; FAM, fast anatomical mapping.

raters. The median rating scores for various LA anatomical structures are as follows: LSPV—2.00/2.00 (IQR 2.00–2.00); LIPV—1.89/2.00 (IQR 1.89–1.91); RSPV—1.82/2.00 (IQR 1.75–1.82); RIPV—1.82/2.00 (IQR 1.82–1.82); LAA—1.75/2.00 (IQR 1.75–1.75), and overall LA body—4.32/5.00 (IQR 4.31–4.32) (*Table 4*). The average min CT registration error was 0 mm, and the average max error was 11.97 mm. No differences between raters were found for all LA adjacent structures and overall LA shell, showing high agreements were reported across the three raters. As shown in *Table 5*, the Kappa coefficients between

Table 5 Correlation of scores (Kappa coefficients) between each pair of raters

LA structure	Rater 1-Rate 2	Rate 2-Rater 3	Rate 3-Rate 1
LSPV	1.00	1.00	1.00
LIPV	1.00	0.78	0.78
RSPV	1.00	0.44	0.45
RIPV	1.00	0.75	0.75
LAA	1.00	0.81	0.81
Overall LA shell	0.68	0.73	0.75

LA, left atrium; LSPV, left superior pulmonary vein; LIPV, left inferior pulmonary vein; RSPV, right superior pulmonary vein; RIPV, right inferior pulmonary vein; LAA, left atrial appendage.

each pair of raters for LSPV, LIPV, RIPV, and LAA were all ≥0.75, indicating strong agreement between all three raters. For RSPV, high agreements were established between Rater 1 and Rater 2, and both Rater 1 and Rater 2 had fair agreements with Rater 3 (Rater 2-Rater 3: $\kappa = 0.44$ and Rater 3-Rater 1: $\kappa = 0.45$). For the overall LA shell, high degrees of agreement were also observed across all raters (Rate 1-Rater 2: $\kappa = 0.68$, Rater 2-Rater 3: $\kappa = 0.73$ and Rater 3-Rater 1: $\kappa = 0.75$).

Discussion

This study evaluates our institution's first human use of ICE to reconstruct LA anatomical shell in 3D from the RA without the use of a multipolar mapping catheter. The use of ICE has become more versatile in the AF ablation workflow. One of the major advantages of using ICE in AF ablations is the significant reduction in the need of fluoroscopy. Fluoroless ablation with ICE have been well described and reported by numerous studies with excellent feasibility, safety, and efficacy.[4,7–9] Most fluoroless ablation techniques rely on manual annotation of the PVs, LAA, CS, oesophagus, etc. through either ICE or electroanatomical mapping (EAM) catheters and integration with CT. In our study, the average fluoroscopy time was 10 ± 8.7 min, and six patients underwent fluoroless ablation. The ability to accurately reconstruct key anatomical structures is critical to a safe and successful AF ablation. However, precise reconstruction of LA anatomy is often influenced by operator experience. AI, especially in the form of DL, is gaining popularity in the field electrophysiology. Deep learning applications in

AF commonly include computational modelling to study AF mechanisms, classify AF risk factors, personalize therapy for patients, automatically identifying ablation targets, etc.[10–15] DL has the ability to not only learn from countless data input to generate reliable and unbiased output but also continue algorithmic optimization in the post-development phase. Automatic detection of LA anatomy by a well-trained AI algorithm has the potential to further streamline the current AF ablation workflow, enhance anatomical accuracy, and improve ablation success and patient outcomes. All 28 patients in our study underwent successful AF ablation, and no immediate post-ablation complications were observed.

To the best of our knowledge, this is the first study that compared LA anatomical structures reconstructed from the DL algorithm with gold-standard cardiac CT in a high-volume US centre. A recently published manuscript investigating the same DL algorithm used ablation catheters to confirm correct identification of structures and automated lesion tag location in relation to PVs generated by the DL algorithm.[16] This study demonstrated that the automated ICE-based algorithm can correctly identify the LA anatomical structures in all patients with relatively high accuracy compared to automated lesion tags for PV segments. However, no direct comparison with CT was reported. Results from our study showed that LA anatomical structures including all four PVs and LAA reconstructed by this DL algorithm had <1–2 mm of difference in ostial diameter compared to pre-procedural CT. The carina-to-carina distance measured between the left and right PVs was also comparable between the DL algorithm and gold-standard CT. Moreover, qualitative evaluation of the DL algorithm integration with ICE catheters by three different electrophysiologists also demonstrated comparable LA images. Integrating DL into the existing imaging system as demonstrated in this study can limit the amount of operator variability and reliably deliver accurate and reproducible anatomical landmarks. In the current practice of AF ablation strategies, PVI is often the only ablation performed in many centres during the first ablation attempt. The ability to obtain LA anatomy automatically through ICE can theoretically reduce both mapping and procedure time and simplify the ablation workflow. While many practices utilize mapping catheter-based EAM to construct the LA shell, in some cases, anatomical accuracy can also be impacted by the amount of contact force (CF) applied to the LA tissue as higher CF can cause structural distortion.[17] This limitation potentially can be better mitigated by the DL algorithm as no catheter-tissue contact is necessary to construct the anatomical shell. Last but not least, it is also important to note that the DL algorithm described in this study selected for frames within the ULS clips that were gated to the end-expiration phase and to the LA max volume. This takes into account prior evidence demonstrating that LA volumes can be more precisely determined through respiratory gating.[18] In addition, with the future advent of pulsed field ablation, the possibility of performing ablation with one trans-septal only might become the standard. This technology will allow a good 3D anatomical shell obtained without the use of a multi-polar mapping catheter. This would be also the case for thermal energy source procedures such as cryoenergy and RF where the ablation targets can be achieved irrespective of voltage information.

From our results, best practice recommendations were also summarized. The required input for the DL algorithm is as follows:

(1) 2D ULS distinct frames, with full spatial coverage of the LA body and its adjacent key anatomical structures including LAA and PVs, with at least two different views for each structure, and preferably clearly visualizing the ostium of the PVs and LAA.
(2) The 2D clips should be acquired while the ICE catheter is positioned in the RA and/or the RVOT.
(3) The selected frames within the ULS clip should be gated at the end-expiration phase and to the LA max volume.
(4) LA frames with a temporal resolution of ~20 ms just before the opening of the mitral valve at the time of maximal atrial volume (end atrial diastole).
(5) The selected frames within the ULS clip should be with depth 90–120 mm.
(6) The LA anatomy should not have uncommon anatomical variation (e.g. 5th PV).
(7) There should not be map shifts between the ULS data (frames) and the magnetic data (FAM, VISITAGs, electroanatomical points, etc.) in the clinical procedure.

Limitations

This study has several limitations. First, this is a single-centre feasibility study, and no comparison group was included in this study design. Second, reproducibility of the study results in other patient cohorts was not tested yet. Moreover, the current version of the DL algorithm is only limited to frames with 90–120 mm depth and patients without anatomical variations such as a 5th PV. Further training of the DL algorithm to accommodate more anatomical variations and improve detection speed and accuracy is desired. Lastly, this algorithm will not provide voltage map data. Prospective studies focusing on both procedure-oriented and outcome-oriented endpoints are needed to further investigate the efficacy of this proposed new DL module.

Conclusion

The DL algorithm integration with ICE catheters demonstrated considerable accuracy compared to cardiac CT and across multiple physician raters with good ablation success and immediate safety. The comparability and feasibility of ICE with this algorithm poses future additional clinical implications. Further studies are required to evaluate the safety and efficiency of this new DL module.

Funding

None declared.

Conflict of interest: L.D.B. is a consultant for Stereotaxis, Biosense Webster, Boston Scientific, Abbott Medical; has received speaker honoraria/travel from Medtronic, Atricure, Biotronik, Baylis Medical, and Zoll. G.H., D.H., R.A.M., J.A., G.C., and R.U. are employees of Biosense Webster, Inc. The remaining authors report no conflict of interest.

Data availability

All relevant data are within the manuscript.

References

1. Antolic B, Kajdic N, Vrbajnscak M, Jan M, Zizek D. Integrated 3D intracardiac ultrasound imaging with detailed pulmonary vein delineation guided fluoroless ablation of atrial fibrillation. *Pacing Clin Electrophysiol* 2021;**44**:1487–96.
2. Nishiyama T, Katsumata Y, Inagawa K, Kimura T, Nishiyama N, Fukumoto K *et al.* Visualization of the left atrial appendage by phased-array intracardiac echocardiography from the pulmonary artery in patients with atrial fibrillation. *Europace* 2015;**17**:546–51.
3. Romero J, Patel K, Briceno D, Alviz I, Tarantino N, Della Rocca DG *et al.* Fluoroless atrial fibrillation catheter ablation: technique and clinical outcomes. *Card Electrophysiol Clin* 2020;**12**:233–45.
4. Ahn J, Shin DG, Han SJ, Lim HE. Safety and efficacy of intracardiac echocardiography-guided zero-fluoroscopic cryoballoon ablation for atrial fibrillation: a prospective randomized controlled trial. *Europace* 2023;**25**:euad086. doi:10.1093/europace/euad086.
5. Saleh M, Coleman KM, Vaishnav AS, Shein J, Makker P, Skipitaris N *et al.* Intracardiac echocardiography guided nonocclusive balloon cryothermal applications to achieve antral isolation during pulmonary vein isolation. *J Interv Card Electrophysiol* Nov 2021;**62**:329–36.
6. Liu X, Lin R, Peng X, Wang X, Li Y, Liu X *et al.* Visualization and mapping of the right phrenic nerve by intracardiac echocardiography during atrial fibrillation ablation. *Europace* 2023;**25**:1352–60.
7. Lurie A, Amit G, Divakaramenon S, Acosta JG, Healey JS, Wong JA. Outcomes and safety of fluoroless catheter ablation for atrial fibrillation. *CJC Open* 2021;**3**:303–10.
8. Lerman BB, Markowitz SM, Liu CF, Thomas G, Ip JE, Cheung JW. Fluoroless catheter ablation of atrial fibrillation. *Heart Rhythm* 2017;**14**:928–34.

9. Liu X, Palmer J. Outcomes of 200 consecutive, fluoroless atrial fibrillation ablations using a new technique. *Pacing Clin Electrophysiol* 2018;**41**:1404–11.
10. Feeny AK, Chung MK, Madabhushi A, Attia ZI, Cikes M, Firouznia M *et al.* Artificial intelligence and machine learning in arrhythmias and cardiac electrophysiology. *Circ Arrhythm Electrophysiol* 2020;**13**:e007952.
11. Saglietto A, Gaita F, Blomstrom-Lundqvist C, Arbelo E, Dagres N, Brugada J *et al.* AFA-recur: an ESC EORP AFA-LT registry machine-learning web calculator predicting atrial fibrillation recurrence after ablation. *Europace* 2023;**25**:92–100.
12. Szymanski T, Ashton R, Sekelj S, Petrungaro B, Pollock KG, Sandler B *et al.* Budget impact analysis of a machine learning algorithm to predict high risk of atrial fibrillation among primary care patients. *Europace* 2022;**24**:1240–7.
13. Hygrell T, Viberg F, Dahlberg E, Charlton PH, Kemp Gudmundsdottir K, Mant J *et al.* An artificial intelligence-based model for prediction of atrial fibrillation from single-lead sinus rhythm electrocardiograms facilitating screening. *Europace* 2023;**25**:1332–8.
14. Luongo G, Vacanti G, Nitzke V, Nairn D, Nagel C, Kabiri D *et al.* Hybrid machine learning to localize atrial flutter substrates using the surface 12-lead electrocardiogram. *Europace* 2022;**24**:1186–94.
15. Leclercq C, Witt H, Hindricks G, Katra RP, Albert D, Belliger A *et al.* Wearables, telemedicine, and artificial intelligence in arrhythmias and heart failure: proceedings of the European Society of Cardiology cardiovascular round table. *Europace* 2022;**24**:1372–83.
16. Akerström F, Drca N, Jensen-Urstad M, Braunschweig F. Feasibility of a novel algorithm for automated reconstruction of the left atrial anatomy based on intracardiac echocardiography. *Pacing Clin Electrophysiol* 2022;**45**:1288–94.
17. Anjo N, Nakahara S, Okumura Y, Hori Y, Nagashima K, Komatsu T *et al.* Impact of catheter tip-tissue contact on three-dimensional left atrial geometries: relationship between the external structures and anatomic distortion of 3D fast anatomical mapping and high contact force guided images. *Int J Cardiol. Nov* 1 2016;**222**:202–8.
18. Khan F, Banchs JE, Skibba JB, Grando-Ting J, Kelleman J, Singh H *et al.* Determination of left atrium volume by fast anatomical mapping and intracardiac echocardiography. The contribution of respiratory gating. *J Interv Card Electrophysiol* 2015;**42**:129–34.